Online Model Based Estimation of Complete Joint Stiffness of Human Arm

Cheng Fang, Arash Ajoudani, Antonio Bicchi, and Nikos G. Tsagarakis

***Abstract*—The endpoint stiffness of the human arm has been long recognized as a key component ensuring the quasi-static stability of the arm physical interactions with the external world. Similarly, the understanding of the joint stiffness behavior can provide complementary insights, e.g., on the underlying stiffness regulation principles across different joints including the nullspace stiffness profiles. Traditionally, the experimental modeling and estimation of the human arm joint stiffness is achieved by the transformation of the identified arm endpoint stiffness to the joint coordinates. Due to the underlying kinematic redundancy, the obtained joint stiffness matrix is rank-deficient which implies that the information in the joint stiffness matrix is incomplete. While in robotics applications this issue can be addressed by designing a desired nullspace stiffness behavior through appropriate projections, the use of a similar technique in the identification of human joint stiffness profile is meaningless. Hence, the first objective of this work is to address this issue by developing a novel technique to identify the complete and physiologically meaningful joint stiffness of human arm. Second, we present a model-based online estimation technique to estimate the seven-dimensional complete joint stiffness in various arm poses and activation levels of the two dominant arm muscles that correspond to the geometric and volume modifications of the joint stiffness profile, respectively.**

***Index Terms*—Calibration and identification, human factors and human-in-the-loop, physical human-robot interaction.**

I. Introduction

WITH robots increasingly entering our workspaces to provide daily service and clinical care, effective and intuitive Human-Robot Interaction (HRI) has become a key component to enhance their cross-application compatibility. A potential way to equip the robots with superior whole-body interaction capabilities is to exploit and integrate the human's underlying sensorimotor principles into their mechanical and control principle designs. In fact, several previous studies in the field of robot interaction control have been inspired by the observations in neuroscience and human biomechanics, some of which can be found in [1]–[3].

The mechanical stability of humans, commonly referred as the ability to regulate the force-displacement relationship at contact(s), has been long recognized as a fundamental component to produce stable and versatile interactions with uncertain environments [2], [4]. Within this context, a considerable amount of effort has been devoted to investigating the ability of humans to regulate the arm endpoint stiffness using pose or muscle activations, with the aim to transfer the underlying principles during interactions to the robotic or assistive platforms [3], [5]. In most cases, the technique for measuring and quantifying the human arm endpoint stiffness is to apply stochastic perturbations to the human hand while measuring the restoring forces, which is followed by a post-processing step to estimate the stiffness behavior in the Cartesian space [4], [6].

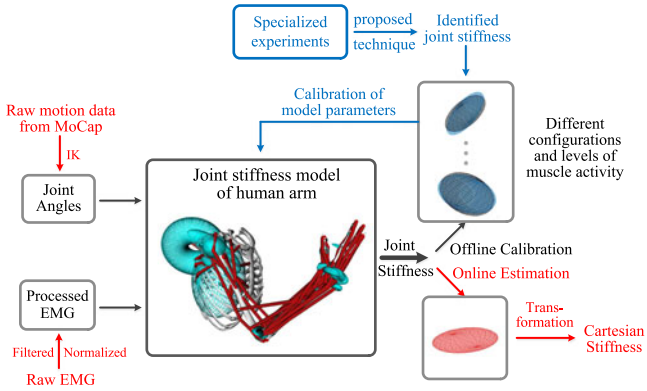

Fig. 1. Schematic diagram of the procedure of the proposed online estimation method for human arm joint stiffness.

In addition to the investigation of the role of Cartesian stiffness in human physical interactions, the analysis of the joint stiffness behaviour of the human arm can provide complementary insights into intuitive regulation of the robot stiffness in the joint coordinates. For example, such principles can be used to achieve a certain nullspace stiffness profile in whole body interaction scenarios that involve multiple contacts between the robot (e.g., humanoid robot, upper body exoskeleton) and the external environment. A large number of pioneering studies have been conducted extensively for identifying the joint stiffness of human arm and understanding its relationship with the arm posture and the muscle activation level under different conditions [7]–[9]. However, in almost all of these researches, human arm was constrained to move on a horizontal plane with fixed wrist joint in order to simplify the arm to a 2-DoF planar arm model and avoid the inherent redundancy problem in the human arm. In this case, the joint stiffness of human arm can be obtained by simply transforming the identified Cartesian stiffness to the joint space (one-to-one mapping), which is infeasible for the 3D complete and redundant 7-DoF human arm model.

Manuscript received February 15, 2017; accepted July 6, 2017. Date of publication July 24, 2017; date of current version August 17, 2017. This letter was recommended for publication by Associate Editor K. Lynch and Editor A. M. Okamura upon evaluation of the reviewers' comments. The work was supported by FP7 European Project, WALK-MAN FP7-ICT-2013-10. *(Corresponding author: Cheng Fang.)*

The authors are with the Department of Advanced Robotics, Istituto Italiano di Tecnologia, Genova 16163, Italy (e-mail: cheng.fang@iit.it; arash.ajoudani@iit.it; antonio.bicchi@iit.it; nikos.tsagarakis@iit.it).

This paper has supplementary downloadable material available at http://ieeexplore.ieee.org.

Digital Object Identifier 10.1109/LRA.2017.2731524

The first contribution of this letter addresses this issue with the introduction of a novel technique to identify the complete ($\in \mathbb{R}^{7\times7}$) and physiologically meaningful joint stiffness of the human arm. Consequently and as an extension to our recent results in online tracking of human arm endpoint stiffness [5], we propose an online model to estimate the complete joint stiffness matrix. Specifically, the arm configuration can be tracked by a motion capture system (MoCap), followed by an inverse kinematics (IK) algorithm, that computes the joint angles of the human arm. The joint angles then form an input for the calculation of the muscle Jacobian, which accounts for the configuration-dependent property of the joint stiffness geometry. Meanwhile, the volume-adjusting component of the joint stiffness is incorporated by the EMG signals of a pair of dominant forearm antagonistic muscles, i.e., Biceps and Triceps. A number of trials can be conducted to estimate a series of realistic joint stiffness matrices in various arm configurations and co-activation profiles of the arm muscles by the proposed technique for the off-line calibration of the joint stiffness estimation model. Afterwards, the calibrated model can be used for online estimation of the joint/Cartesian stiffness. The whole procedure of the method is illustrated in Fig. 1. Such model can offer deep insights into the underlying stiffness regulation principles in human arms and provide guidelines both for the design and control of emerging impedance regulation capable robotic manipulators/humanoids towards the teleoperation or autonomous applications of performing whole body physical interaction tasks.

II. Identification of the Joint Stiffness/Compliance of Human Arm

A. Strategy of the Identification

The *Conservative Congruence Transformation* (CCT) from the Cartesian stiffness, K_C, to the joint stiffness, K_J, without the consideration of the external load can be written[1]:

$$K_J = J^T(q)K_C J(q). \tag{1}$$

Using such a technique, the arm stiffness information is transformed from the Cartesian space ($\in \mathbb{R}^{6\times6}$) to a larger joint space ($\in \mathbb{R}^{n\times n}$, $n > 6$ in redundant cases), therefore the obtained joint stiffness matrix is rank-deficient which implies that the information in the joint stiffness matrix is incomplete. For instance, human arm can be modelled by 7 degrees of freedom (DoF), the derived stiffness information from a symmetrical 6×6 Cartesian stiffness matrix is not sufficient for a complete symmetrical 7×7 joint stiffness matrix. The lost 7-DoF (containing 7 independent variables, due to the symmetric properties of the matrices) information could be defined as the nullspace stiffness with respect to the Cartesian stiffness, K_N [11].

The design of the nullspace stiffness behaviour in robotics is achieved by projecting an arbitrary 7×7 stiffness matrix using a dynamically consistent projector. The goal in such applications are to perform a secondary task which does not affect the dynamic behaviour at the end-effector [12]. Therefore, the design of the complete joint stiffness of the robotic arm can be done by combining the joint stiffness component of (1) and the nullspace stiffness component, K_N. The application of a similar technique to the human arm will be mathematically meaningful, but will be most likely to result in wrong and misleading values of the nullspace stiffness with respect to the Cartesian stiffness of the human arm, which can be identified through the classical perturbation experiments [13]. The discrepancy between the robotic arm and the human arm regarding the stiffness problem is caused by the fact that the former is a design problem while the latter is an identification problem. Fig. 2(a) shows the drawback of the identification method of the human arm joint stiffness by using the traditional stiffness transformation (1). Therefore, one of the main goals in this letter is to develop a novel technique to identify the actual complete joint stiffness of the human arm.

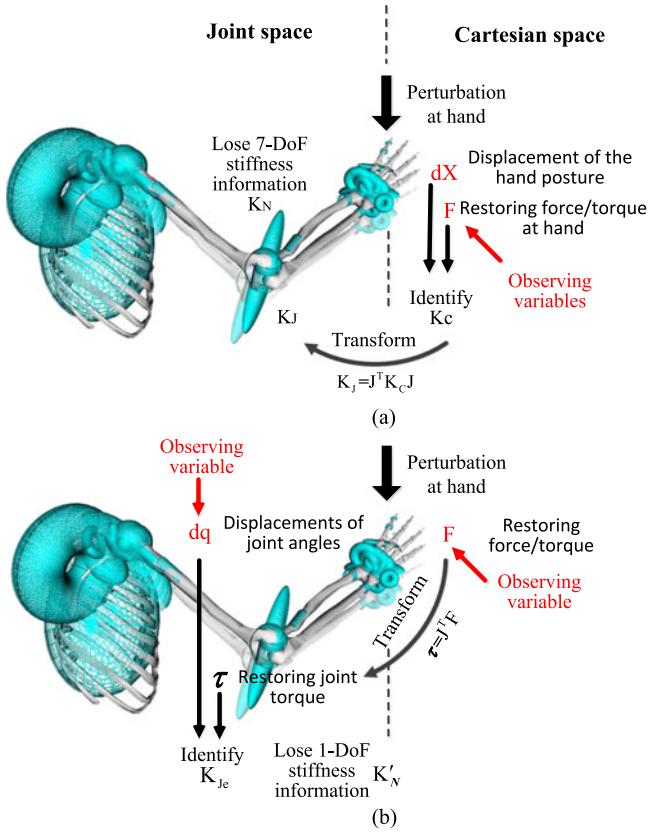

Fig. 2. Two different potential strategies for identifying the joint stiffness of human arm: (a) the traditional strategy, (b) the proposed strategy in this letter.

To do so, we apply perturbations to the hand in Cartesian space and observe the effects in joint space. By measuring the human kinematics during perturbations (e.g., using a MoCap system and an IK algorithm for calculating the joint angles of human arm model), we will be able to observe the joint displacements, dq, directly. Meanwhile, the measured forces and torques F at hand can be transformed to the joint torques τ, using $\tau = J^T(q)F$, with $J^T(q)$ being the arm Jacobian transpose. Finally, similar to classical techniques [13], the identification of a joint stiffness matrix, K_{Je}, can be achieved using dq and τ. It is important to note that the identified result is not the ground truth of the human arm joint stiffness since all the input torques are from the range of the transpose of the Jacobian, $R(J^T)$, which is a subspace of the whole joint torque space, $\mathbb{R}^7$. Due to this limitation, 1-DoF stiffness information is still lost. Nevertheless,

[1]The item in CCT, $\frac{\partial J^T(q)}{\partial q} f$, capturing the effect of arm geometry in the presence of external load, f, can be safely neglected since the external force will not be considered in this letter [10].

it is worth noting that the human arm stiffness behavior is observed and identified in the joint space instead of the traditional Cartesian space in this way, and the estimate of the joint stiffness is much closer to the realistic joint stiffness of human arm since only 1-DoF stiffness information is missing. This 1-DoF nullspace stiffness, $K_N^{'}$ is defined as a new nullspace stiffness with respect to the estimate of the joint stiffness, K_{Je}, which means the component of the human arm joint stiffness, $K_N^{'}$, is fully decoupled from K_{Je}. Therefore, this technique results in the identification of the 1-DoF nullspace stiffness $K_N^{'}$ instead of the 7-DoF K_N. Note that these two nullspace stiffnesses are defined with respect to different reference stiffnesses, K_C and K_{Je}. Fig. 2(b) shows the proposed strategy for identifying the whole joint stiffness of human arm.

Next, for the sake of convenience of expression and explanation, the compliance terminology will be mainly used as the dual quantity of the stiffness (compliance is the inverse of the corresponding stiffness, i.e., $C_C = K_C^{-1}$, $C_J = K_J^{-1}$). Accordingly, the corresponding nullspace compliance $C_N^{'}$ is defined as:

$$C_J = C_{Je} + C_N^{'}, \tag{2}$$

and the structure of $C_N^{'}$ will be explored and investigated. C_{Je} is the identified joint compliance by using the proposed method shown in Fig. 2(b).[2] $C_N^{'}$ is the component which is not observable when identifying C_{Je}, which means that all the joint displacement responses of this compliance component, $C_N^{'}$, to the restoring torques caused by the perturbation at the hand will always be zeros. This fact can be formulated mathematically as follows:

$$\begin{aligned}&(C_{Je} + C_N^{'})J^T F = C_{Je}J^T F \ \ (\forall F \in \mathbb{R}^6) \ \Rightarrow \\ &C_N^{'}J^T = O \ \Rightarrow \\ &\begin{pmatrix} U_1 & U_2 & \cdots & U_7 \end{pmatrix} \begin{pmatrix} \sigma_1 & & & \\ & \sigma_2 & & \\ & & \ddots & \\ & & & \sigma_7 \end{pmatrix} \begin{pmatrix} U_1^T \\ U_2^T \\ \vdots \\ U_7^T \end{pmatrix} J^T = O.\end{aligned} \tag{3}$$

Since $C_N^{'}$ is symmetrical, its singular value decomposition can be expressed as in (3). To make (3) hold for any restoring force/torque at hand, F, the only way is to make all the projections of the columns of J^T on the eigenvectors (U_i) corresponding to the non-zero eigenvalues (σ_i) equal to zeros. In this case, the only possibly desirable eigenvector is the basis vector of the nullspace of the Jabocian $(N(J))$, V. Therefore, $C_N^{'}$ can be rewritten as:

$$C_N^{'} = \sigma_n V V^T. \tag{4}$$

Here, σ_n $(\in \mathbb{R}$, considering 7-DoF human arm) indicates the magnitude of the nullspace compliance, $C_N^{'}$, along the V-direction, which is the lost 1-DoF compliance information after identifying C_{Je}. Its intuitive meaning is illustrated in Fig. 3 by reducing the dimension from 7 to 3 for visualization purpose.

[2]The identified K_{Je} usually has full rank which is observed and verified in the real identification results. Therefore, we have $C_{Je} = K_{Je}^{-1}$.

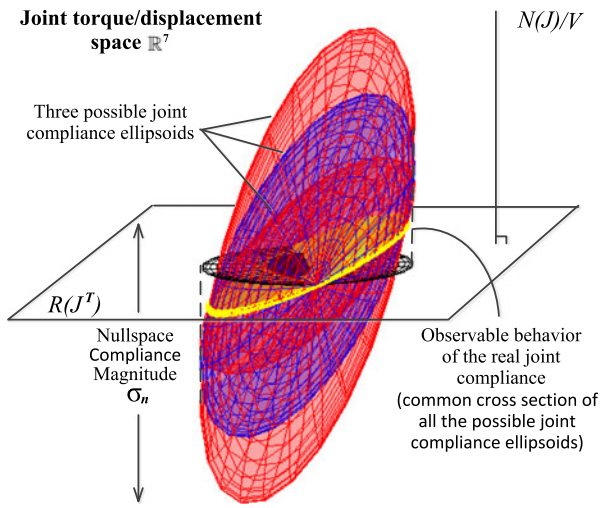

Fig. 3. Explanation on the nullspace compliance of human arm. The symmetric joint stiffness can be represented by a hyperellipsoid, but the normal ellipsoid is employed here only for explanatory purpose.

The yellow elliptic cross section in Fig. 3 is the observable behavior of the joint displacement responses to the constrained restoring joint torques on the subspace $R(J^T)$ with unit magnitude. It is the common cross section of all the possible compliance ellipsoids of human arm with different nullspace compliance magnitudes (such as the two red ellipsoids and one blue ellipsoid).[3] This property is reflected by (3) and (4). Therefore, the whole geometry of the real joint compliance ellipsoid (the projection of the ellipsoid on $N(J)$ specifically) can not be observed and determined directly due to the impossibility of introducing the stimulating torque components in the V-direction. Accordingly, some special supplementary experiment needs to be designed to estimate the only lost compliance information, σ_n, the nullspace compliance magnitude along the V-direction, to reveal the realistic joint compliance:

$$C_J = C_{Je} + \sigma_n V V^T. \tag{5}$$

B. Design of the Identification

In this section, a two-stage identification procedure is designed to estimate the complete joint stiffness of human arm according to the structure of the joint compliance shown in (5). To identify σ_n, the basic idea is to change the structural property of the human arm in a way that the influence of σ_n could flow out to the hand to become observable.

In the first stage, only 1-DoF shoulder-hand rotational perturbations (rotational displacements with stochastic magnitudes at hand about the same direction connecting the center of the shoulder and the point of the hand at which perturbations are applied)[4] would be applied at the hand of a subject who wears

[3]The compliance ellipsoid of human arm is generated by all the joint displacement responses of C_J to any stimulating joint torques of unit magnitude in the whole space $\mathbb{R}^7$.

[4]The reason for the special design is that only 2-DoF motion at hand is left for the 5-DoF constrained arm, which is caused by the composition of the arm self-rotation about the shoulder-hand direction and the self-rotation of the forearm, after the 3-DoF position of the hand is constrained by the handle, which the hand has to grip firmly for the perturbation experiment.

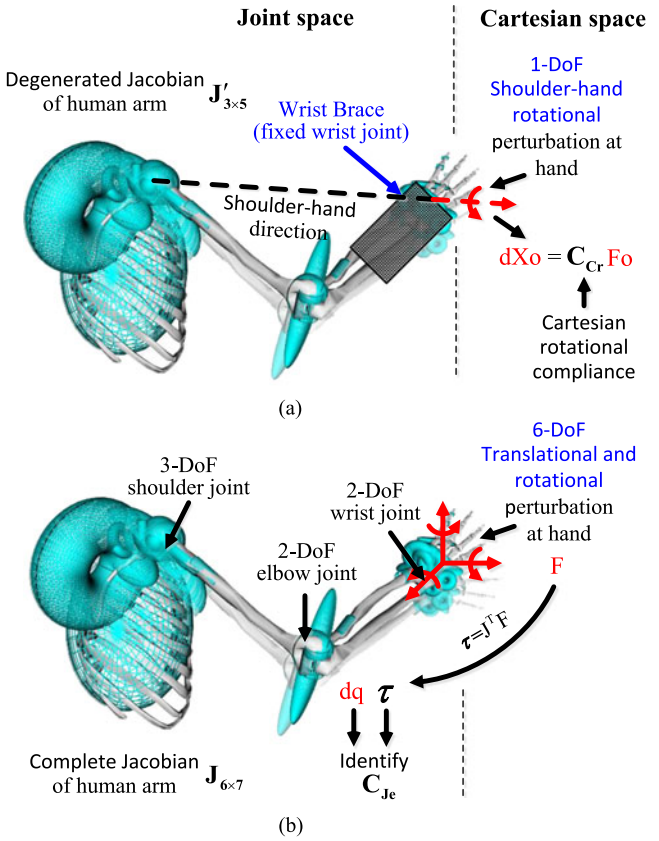

Fig. 4. The two-stage indentification procedure: (a) In the first stage, only 1-DoF shoulder-hand rotational perturbations are applied at the hand while wearing a wrist brace. (b) In the second stage, 6-DoF translational and rotational perturbations are applied without the wrist brace. (Red variables stand for the observed variables).

a wrist brace to fix his/her wrist joint [see Fig. 4(a)]. In the second stage, the full 6-DoF translational and rotational perturbations will be exerted at the same place, and the wrist brace will be removed to have the wirst joint free during this stage [see Fig. 4(b)]. The arm posture and the muscle activation level must be kept consistent in both stages as much as possible. In fact, the whole identification is a continuous process. Thirty five seconds (35 s) are assigned to each perturbation stage and 30 s are designed between these two stages as a break period to have the wrist brace removed.

In the second stage, the joint torque, τ, calculated from the observed restoring 6-dimensional force/torque at the hand, F, and the observed joint angle displacement, dq, can be employed to identify C_{Je} in (5) by using a frequency domain identification technique [13]. The first stage of the perturbation experiment is actually the supplementary part which is designed to assist in the identification of the unobservable nullspace compliance, C'_N. In this stage, the dimension of the relevant kinematic Jacobian of the constrained arm, J', is reduced from 6×7 to 3×5 due to the fixed wrist joint:

$$\begin{aligned} J' &= S_1 J S_2 \\ S_1 &= [O_{3\times3}\ I_3]\ S_2 = [I_5\ O_{5\times2}]^T, \end{aligned} \tag{6}$$

where selection matrices S_1 and S_2 are used to select the first five columns of the orientation part of the original Jacobian, J, to form the new Jacobian, J'. The last two columns corresponding to the wrist joint are removed in this case. $O_{m\times n}$ means the $m \times n$ zero matrix and I_n indicates the identity matrix of size n. Meanwhile, the complete joint compliance of the human arm in the second stage, C_J, is degenerated into the joint compliance in the first stage, C'_J, as below under the assumption that all the factors contributing to the joint compliance will be kept unchanged:

$$C'_J = S_2^T C_J S_2, \tag{7}$$

which means all the elements relevant to the wrist joint (the last two rows and columns) in the original joint compliance matrix, C_J, will be eliminated by the selection matrix, S_2. With all these changes to the arm kinematic Jacobian and the arm joint compliance, we could have this relationship:

$$C_{C_r} = J' C'_J J'^T, \tag{8}$$

where C_{C_r} is the Cartesian rotational compliance matrix of the constrained arm in the first stage. Together with (5), (6), and (7), we have:

$$C_{C_r} = S_1 J S_2 S_2^T (C_{J_e} + \sigma_n V V^T) S_2 S_2^T J^T S_1^T. \tag{9}$$

In this stage, the measured and observed rotational displacement, dX_O, and the restoring torques, F_O, at hand can be used to identify the corresponding restoring torque, $\hat{F_O}$, for the unit rotational displacment, $d\hat{X}_O$, which is the shoulder-hand direction. Therefore, we have the following:

$$d\hat{X}_O = [S_1 J S_2 S_2^T (C_{J_e} + \sigma_n V V^T) S_2 S_2^T J^T S_1^T] \hat{F_O}, \tag{10}$$

and the estimate of the nullspace compliance σ_{n_e} can be identified by minimizing the Euclidean norm:

$$\begin{aligned} \sigma_{n_e} = \underset{\sigma_n}{\operatorname{argmin}} \| d\hat{X}_O - [S_1 J S_2 S_2^T (C_{J_e} + \sigma_n V V^T) \\ \times S_2 S_2^T J^T S_1^T] \hat{F_O} \|. \end{aligned} \tag{11}$$

Eventually, the whole joint stiffness of human arm can be identified and calculated by[5]:

$$K_J = (C_{J_e} + \sigma_{n_e} V V^T)^{-1}. \tag{12}$$

III. Joint Stiffness Estimation Model of Human Arm

As introduced in the preceding section, the direct way of estimating the realistic and subject-specific human arm joint stiffness matrix is a two-phase perturbation-based process. Nevertheless, such a technique imposes severe constraints to the limbs, making it not suitable for the online task execution scenarios. Hence, a model has to be proposed to account for the identified joint stiffnesses (off-line calibration) and estimate the different joint stiffnesses in different conditions in real time (online application).

It is well known that the joint stiffness of human arm is physiologically produced by the muscle stiffness with the transformation [14]:

$$K_J = J_M^T(q) K_M J_M(q), \tag{13}$$

[5]Please refer to [11] for the calculation of V.

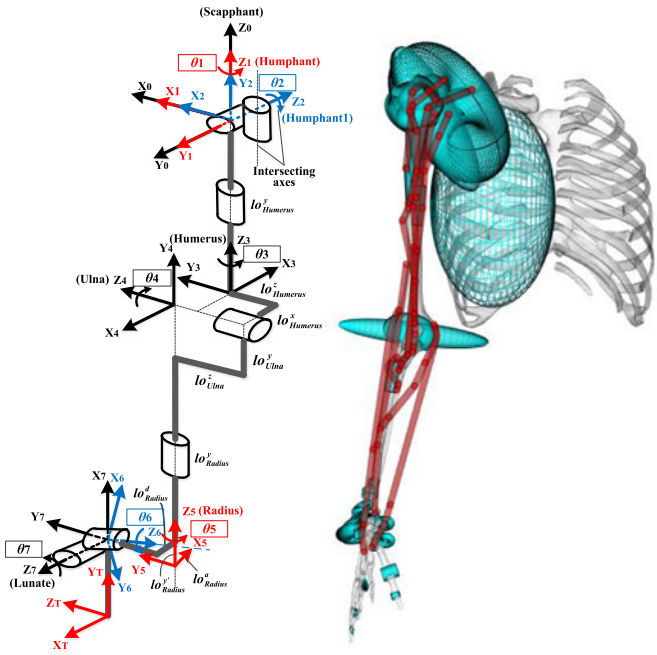

Fig. 5. Musculoskeletal model of human right arm with principal muscles and its corresponding kinematic model in the modified Denavit-Hartenberg notation.

where the muscle stiffness, K_M, is a $m \times m$ diagonal matrix, and m is the number of involved muscles. Each element of the matrix represents the stiffness of a specific muscle. The muscle Jacobian, J_M, is a matrix of partial derivatives that relates small muscle length changes with the small joint angle changes $\frac{\partial l_i(q)}{\partial q_j}$, i.e., muscle moment arm:

$$J_M(q) = \begin{pmatrix} \frac{\partial l_1(q)}{\partial q_1} & \frac{\partial l_1(q)}{\partial q_2} & \cdots & \frac{\partial l_1(q)}{\partial q_7} \\ \frac{\partial l_2(q)}{\partial q_1} & \frac{\partial l_2(q)}{\partial q_2} & \cdots & \frac{\partial l_2(q)}{\partial q_7} \\ \vdots & \vdots & \ddots & \vdots \\ \frac{\partial l_m(q)}{\partial q_1} & \frac{\partial l_m(q)}{\partial q_2} & \cdots & \frac{\partial l_m(q)}{\partial q_7} \end{pmatrix}. \quad (14)$$

For computing the elements of $J_M(q)$, a widely used 3-dimensional musculoskeletal model is exploited for locating the relevant muscles [15] as shown in Fig. 5. The configuration of the model (the set of seven joint angles) can be retrieved online by an analytical inverse kinematics algorithm [16].[6] Once the configuration is identified, all the muscle path points can be located correspondingly, and the muscle moment arms can be calculated numerically or analytically. According to the suggestion described in [17], 12 principal muscles, which mostly contribute to the muscle moment arms of the human arm, are selected: the anterior (DELT1) and posterior (DELT3) potions of the Deltoid, the long (BIClong) and short (BICshort) potions of Biceps, Brachialis (BRA), Brachioradialis (BRD), the lateral (TRIlat) and long (TRIlong) portions of Triceps, the Supinator (SUP), the Extensor carpi radialis longus (ECRL), the Flexor carpi radialis (FCR) and the Pronator teres (PT), which are presented in Fig. 5.

[6]This can be also realized by the built-in IK in the OpenSim software.

The muscle stiffness matrix K_M in (13) is commonly estimated by using Hill's activation dynamic model with the muscle activities as inputs, which are usually measured by the electromyography signals (EMGs). This, however, requires that the EMG activities of several muscles are measured, processed and fed into a computationally complex and expensive dynamic system of equations for the implementation [18]. On the other hand, a dense body of literature gives solid evidence on the existence of synergistic relationships between the arm mono- and bi-articular muscle activities which achieve a coordinated stiffening profile across the arm joints [19], [20], and as a result of this, strong linear correlations between the level of the synergistic muscle activities and the volume of the arm endpoint stiffness can be observed [3].

Based on these observations, to simplify the muscle activation model, we presume that i) there exists a synergistic relationship between the arm muscle activities, and ii) each muscle activation contributes to its muscle stiffness and the resulting arm stiffness (joint/Cartesian stiffnesses) with a different ratio. Therefore, a simplified muscle stiffness estimation model is proposed as below:

$$\begin{aligned} K_M &= a_{cc} K_S \\ a_{cc} &= c_1 + c_2(p_B + p_T), \end{aligned} \quad (15)$$

where K_S is a time-invariant diagonal matrix which embodies the different capabilities of the muscles for generating muscle stiffness with the same muscle activity. a_{cc} is an index to reflect the level of the synergistic muscle activation. In this study, as the dominant and easily accessible muscles of the arm for surface EMG measurements, the EMG activities of the Biceps p_B and Triceps p_T are used to estimate a_{cc} by formula (15). The internal constant coefficients c_1 and c_2, together with the elements of K_S, are identified experimentally during the off-line calibration phase. Therefore the joint stiffness estimation model of human arm can be derived by combining (13) and (15):

$$K_J = J_M^T(q) a_{cc} K_S J_M(q). \quad (16)$$

Needless to say, the simplified joint stiffness model of human arm is certainly subject to modelling uncertainties and inaccuracies due to the simplifications in the muscle stiffness model and the selection of the principal muscles. However, the main purpose of this research is to provide a computationally efficient method for online complete joint stiffness estimation of human arm towards the robotic applications where the compromise can be tolerated between the calculation efficiency and the modelling accuracy. This conception of the arm stiffness modelling was already proved to be feasible and effective in our previous work [5], [21]. Compared to our previous work, the arm stiffness estimation model is extended from the Cartesian space to the joint space in order to preserve full arm stiffness information. Accordingly, more muscles, especially the muscles spanning more than one joint, are added into the musculoskeletal model to try to interpret the identified joint stiffnesses better.

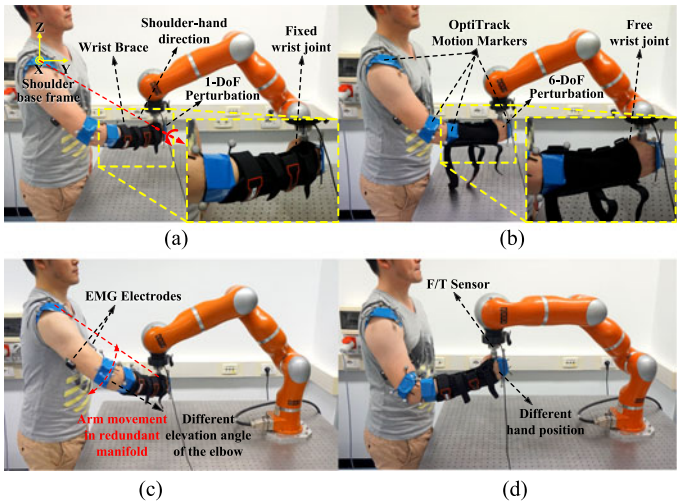

Fig. 6. The experimental setup of the joint stiffness identification of human arm. (a) The first stage of the two-stage identification. Only 1-DoF shoulder-hand rotational perturbations were applied with a wrist brace. (b) The second stage of the two-stage identification. 6-DoF translational and rotational perturbations were applied without the wrist brace effect. The two-stage identification experiment was run in (c) different configurations in terms of different elevation angles of the elbow and (d) different positions of the hand.

IV. Experiments on Human Arm Joint Stiffness

A. Experimental Procedures

This section describes the procedure to identify the parameters in the joint stiffness estimation model, which are 12 elements in K_S, and c_1 and c_2 in a_{cc}.

K_J is measured and identified by the two-stage perturbation experiment introduced in Section II. In the first stage of the experiment [Fig. 6 (a)], after locating the shoulder base frame by the OptiTrack motion capture system, the 1-DoF rotational perturbations, dX_O, about the shoulder-hand direction were applied by a KUKA lightweight robot IV under position control mode to the human hand and the 3-dimensional restoring torques, F_O, were recorded using a 6-axis F/T sensor (ATI Inc.), which was placed between the robot and the handle. In this stage, a wrist brace (ORTHOSERVICE Inc.) was employed to fix the wrist joint. In the second stage [see Fig. 6 (b)], the 6-DoF stochastic translational and rotational perturbations were simultaneously applied by the KUKA robot at the same place with the same arm configuration. The 6-dimensional restoring forces and torques, F, were recorded and transformed into the joint space to calculate the corresponding joint torques, τ. The joint displacement, dq, was observed by the OptiTrack. In this stage, the wrist brace was loosened and pulled a little upward to have the wrist joint completely free. Throughout the whole two-stage identification process, the mean of two processed EMG signls from Biceps and Triceps, $(p_B + p_T)/2$, was displayed back to the subject to help him/her sustain the muscle activation level as steady as possible. By using the method proposed in Section II, the complete joint stiffness of human arm, K_J, can be estimated.

To identify the internal parameters of the joint stiffness estimation model of human arm, K_J must be identified in different arm configurations and muscle activation levels. The two-stage identification experiment was carried out in eight different positions of the hand w.r.t the shoulder base frame [see typical example in Fig. 6 (d)]. These positions were chosen anterior to the coronal plane of the body, within a reasonable workspace of the human arm while avoiding singular configurations and joint limits. In each hand position, arm joints were allowed to vary within the redundant manifold of the corresponding shoulder-hand position to achieve three distinct elevation angles of the elbow joint [see typical example in Fig. 6 (c)], resulting in 24 arm configurations in total. At each configuration, the subjects were asked to modulate and keep the activation of the arm muscles in three different levels: minimum-activity, medium and high (see details at [5], [22]).

In the end, all the identified complete joint stiffness matrices in different arm configurations and muscle activation levels during the off-line calibration phase were used to estimate K_{Se}, c_{1e}, and c_{2e} by minimizing the sum of the ratios of the Frobenius norms:

$$\underset{K_S,c_1,c_2}{\operatorname{argmin}} \sum_{i=1}^{n_C} \frac{\| {J_M^i}^T a_{cc}^i(c_1,c_2) K_S J_M^i - K_J^i \|_F}{\| K_J^i \|_F}, \tag{17}$$

with $J_M^i \in \mathbb{R}^{12\times 7}$, $K_S \in \mathbb{R}^{12\times 12}$ and $K_J^i \in \mathbb{R}^{7\times 7}$. The total number of the trials was divided into the calibration trials (n_C) and the test trials (n_T) for the validation of the identified model. Once the model parameters are identified, (16) can be utilized for the online estimation of the arm joint stiffness profile using EMG signals of one antagonistic pair of muscles and the tracking of the arm configuration. In addition, the Cartesian stiffness can be also estimated online easily by using the transformation, $K_C = (J {K_J}^{-1} J^T)^{-1}$.

B. Results

The results of the off-line calibration and the online joint stiffness estimation model for two healthy subjects (male, ages: 33 and 35) are presented in this section.

1) Identification of Complete Joint Stiffness: In all trials, the positive definiteness and symmetric measures of the estimated stiffness/compliance matrices were employed to evaluate the results [5], [13]. Those trials which did not satisfy the above conditions were discarded and repeated.

For better visualization and understanding, the identified joint stiffness from the second stage, K_{J_e}, and the identified complete joint stiffness, K_J, are divided into several 3-dimensional submatrices and subvectors as follows:

$$K = \begin{pmatrix} K_{ss_{3\times 3}} & K_{es_{3\times 1}} & K_{ws_{3\times 3}} \\ K_{se_{1\times 3}} & K_{ee_{1\times 1}} & K_{we_{1\times 3}} \\ K_{sw_{3\times 3}} & K_{ew_{3\times 1}} & K_{ww_{3\times 3}} \end{pmatrix}_{7\times 7}, \ (K = K_{J_e} \text{ or } K_J). \tag{18}$$

It is known that the first three joints of the human arm model are relevant to the physiological shoulder joint (s), and the last three joints can be grouped and considered to be the physiological wrist joint (w), and the remaining fourth joint is the physiological elbow joint (e).[7] Therefore, the 3-dimensional matrix components, K_{ss} and K_{ww}, and the scalar, K_{ee}, in (18) mean

[7]The one degree of freedom of the forearm Pronation/Supination of the elbow can be considered to belong to the wrist joint for better expression.

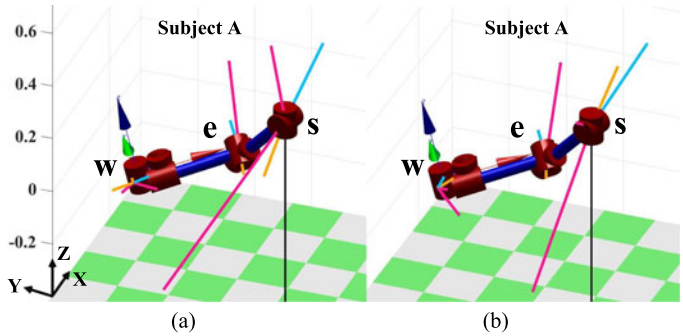

Fig. 7. A visualization example of the identified joint stiffnesses from the proposed two-stage identification method. (a) Identified joint stiffness in the second stage only, K_{J_e}. (b) Estimated complete joint stiffness from the whole two-stage procedure, K_J. Pink (**s**houlder), light blue (**e**lbow), and golden (**w**rist) line segments stand for featured directions of the identified stiffness components which reflect the effects of the shoulder, elbow, and wrist joints on all the physiological joints respectively. The scalings of the line segments at the shoulder, elbow, and wrist joints are 0.008, 0.008, and 0.024 respectively.

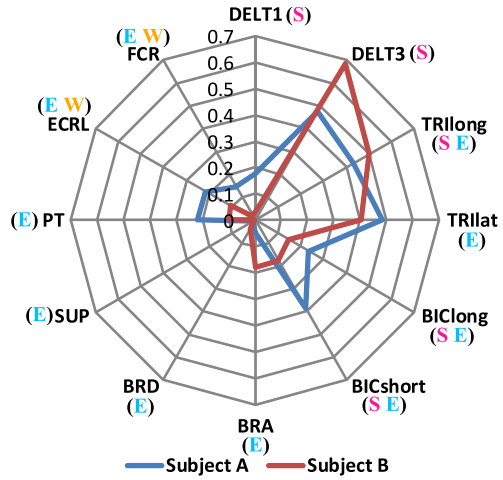

Fig. 8. The distribution chart of the identified stiffnesses (normalized) of the twelve involved arm muscles for subjects A and B. The letters in the parentheses represent the corresponding physiological joints which the muscle spans.

the relative rotational stiffnesses of the shoulder, wrist, and elbow joints respectively (single-joint stiffnesses). The rest of the components reflect the cross coupling effects between different physiological joints (cross-joint stiffnesses). The scale of K_{ee} can be described by the length of a line segment aligned with the rotational axis of the elbow. K_{ss} and K_{ww} can be expressed by their eigenvectors which reveal the featured directions that one needs to make maximum, intermediate, or minimum effort (torque) to move the shoulder or wrist joint about. However, it is worth noting that the eigenvectors of K_{ss} or K_{ww} are expressed in the joint space which need to be transformed to the Cartesian space for visualization. Assume α_{ss}^i and α_{ww}^i $(i = 1, 2, 3)$ are the eigenvectors of K_{ss} and K_{ww} respectively, they can be transformed by:

$$\begin{aligned} \bar{\alpha_{ss}^i} &= J_s \alpha_{ss}^i \\ \bar{\alpha_{ww}^i} &= J_w \alpha_{ww}^i, \end{aligned} \tag{19}$$

in which $\bar{\alpha_{ss}^i}$ and $\bar{\alpha_{ww}^i}$ are the expressions of the eigenvectors in Cartesian space. J_s and J_w consist of the first three columns and the last three columns of J_O respectively, which actually stand for the rotational axis directions of the first three and the last three joints. Through the vector composition, the featured directions of K_{ss} and K_{ww} can be visualized in Cartesian space. Similar operations can be also applied to the remaining components in (18).[8] Fig. 7 illustrates an typical example of the identified joint stiffnesses of the human arm of subject A at the configuration shown in Fig. 6(a). Fig. 7(a) visualizes all the featured directions of the identified K_{J_e} from the second stage, while Fig. 7(b) visualizes the counterpart of the complete joint stiffness K_J calculated from (12) after estimating the nullspace compliance from the optimization (11) ($\sigma_{n_e} = -3.953$(unit:Nm) in this case). Pink (shoulder), light blue (elbow), and golden (wrist) line segments reflect the effects of the corresponding joint on all the physiological joints. For instance, the featured pink vectors of K_{ss}, K_{se}, and K_{sw} are placed at the shoulder, elbow, and wrist joints respectively to reflect the single-joint and cross-joint stiffnesses of the shoulder. Note that those line segments of eigenvectors are usually not orthogonal due to the space transformation. Some obvious difference between the two identified joint stiffnesses can be observed in Fig. 7.

2) Online Joint Stiffness Estimation: In a post processing phase, to evaluate the accuracy of the identified model parameters, the group of test trials (n_T) were used to calculate the average error value between the desired joint stiffness K_J^i identified from the two-stage experiment and the estimate of the online model receiving the same arm configuration q and the muscle activation level p by using:

$$e_T = \frac{\sum_{i=1}^{n_T} \frac{\|J_M^{i\,T}(q)a_{cc}^i(c_{1e},c_{2e},p)K_{Se}J_M^i(q) - K_J^i\|_F}{\|K_J^i\|_F}}{n_T}, \tag{20}$$

which led to the values of 19.8% and 21.6% for subjects A and B respectively. The error is believed to be mainly caused by the simplification in the arm musculoskeletal model. For example, none of the chosen muscles can account for the cross-coupling effects between the shoulder and the wrist, which were observed in our experiments. According to our joint stiffness estimation model (16), the size of the joint stiffness is mainly determined by the index, a_{cc}, (describing the muscle activity) and the size of each element in K_S, and the orientation or pattern of the joint stiffness is regulated by the arm configuration, J_M, and the direction of the identified muscle stiffness index vector, $K_s(K_S = diag(K_s))$. In order to visualize the direction of the vector, we can have:

$$\hat{K_s^A} = K_s^A / \|K_s^A\|, \ \hat{K_s^B} = K_s^B / \|K_s^B\|, \tag{21}$$

where the superscript indicates the corresponding subject. The normalized vectors, $\hat{K_s^A}$ and $\hat{K_s^B}$, can be shown in radar chart in Fig. 8, which reflects the stiffness distribution among different muscles in two subjects. The angle between these two unit vectors is 25.03° $(arccos(\hat{K_s^A}^T \hat{K_s^B}))$. This result implies that the

[8]It is important to note that the input and output vectors of the off-diagonal submatrices in (18) are from different joint subspaces. For example, the input vector of K_{ws} is from the subspace spanned by q_5, q_6, and q_7 and its output vector belongs to the subspace spanned by q_1, q_2, and q_3. In this case, the expressions of the eigenvectors of K_{ws} in Cartesian space are actually the eigenvectors of the matrix, $J_s K_{ws} J_w^{-1}$, which indicate the directions about which the wrist would induce the maximum, intermediate, or minimum resistance from the shoulder if one moves the wrist.

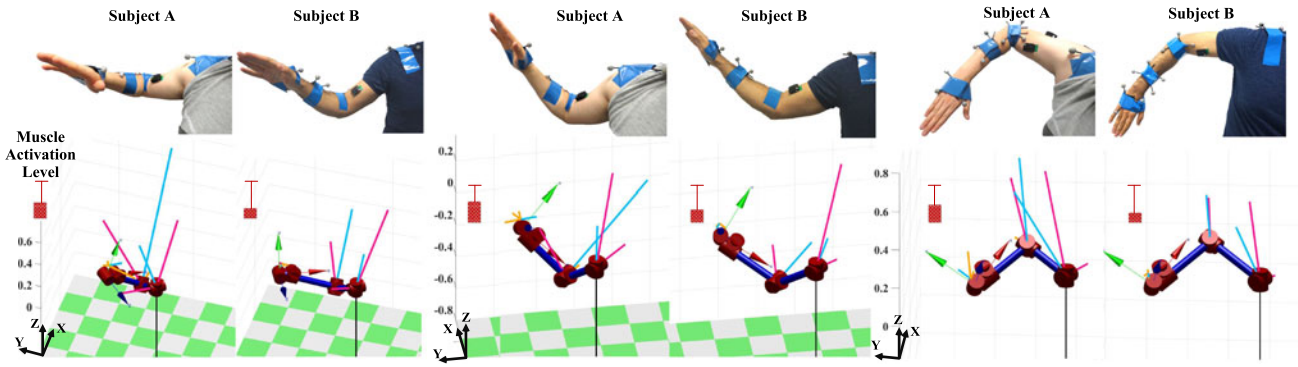

Fig. 9. Online estimation of human arm joint stiffness of subjects A and B at three different configurations (the configurations of the two subjects in each group are very close but not exactly the same). Upper pictures show the real configurations of the human arms. The lower diagrams display all the related featured vectors of the estimated joint stiffness matrices for the corresponding arm state shown above. The scalings of the vectors at the shoulder, elbow, and wrist joints are 0.004, 0.004, and 0.012 respectively for better visibility.

distribution of the arm muscle stiffnesses of healthy subjects tend to have the similar "pattern" (this preliminary result will be further evaluated on more subjects). The pattern reflects muscular synergies in stiffness coordinates which was suggested by some early work as well [9], [19]. The similarity of the identified unit muscle stiffness vector, $\hat{K}_s$, would make the resultant joint stiffnesses of different subjects at the same configuration have the similar "shape" as well. Fig. 9 illustrated the estimation results of the calibrated online models at three different arm postures for the two subjects (see attached video for details).

V. Conclusion

In this letter, we introduced a novel method to online model and estimate the complete human arm stiffness. Such a method can be used not only to monitor the arm stiffness with direct application to teleoperation control but also to study and extract the principles behind stiffness regulation in humans to guide the designs of the autonomous stiffness regulation controllers for robots executing whole body physical interaction tasks, which is our future' work.

The limitation of the proposed two-stage identification method is that the joint stiffness at the configurations with large Flexion/Extension and/or Adduction/Abduction angle(s) of the wrist can not be identified due to the fixation operation of the wrist in the first stage of the identification.

Acknowledgment

The authors would like to thank Dr. L. Peternel for his help in the preparation of the experimental setup.

References

[1] A. Ajoudani, *Transferring Human Impedance Regulation Skills to Robots*. New York, NY, USA: Springer, 2016.
[2] H. Gomi and R. Osu, "Task-dependent viscoelasticity of human multijoint arm and its spatial characteristics for interaction with environments," *J. Neurosci.*, vol. 18, no. 21, pp. 8965–8978, 1998.
[3] T. E. Milner, "Contribution of geometry and joint stiffness to mechanical stability of the human arm," *Exp. Brain Res.*, vol. 143, no. 4, pp. 515–519, 2002.
[4] F. A. Mussa-Ivaldi, N. Hogan, and E. Bizzi, "Neural, mechanical, and geometric factors subserving arm posture in humans," *J. Neurosci.*, vol. 5, no. 10, pp. 2732–2743, 1985.
[5] A. Ajoudani, C. Fang, N. G. Tsagarakis, and A. Bicchi, "A reduced-complexity description of arm endpoint stiffness with applications to teleimpedance control," in *Proc. 2015 IEEE/RSJ Int. Conf., Intell. Robots Syst.*, 2015, pp. 1017–1023.
[6] F. Lacquaniti, M. Carrozzo, and N. Borghese, "Time-varying mechanical behavior of multijointed arm in man," *J. Neurophysiol.*, vol. 69, no. 5, pp. 1443–1464, 1993.
[7] J. McIntyre, F. Mussa-Ivaldi, and E. Bizzi, "The control of stable postures in the multijoint arm," *Exp. Brain Res.*, vol. 110, no. 2, pp. 248–264, 1996.
[8] H. Gomi and M. Kawato, "Human arm stiffness and equilibrium-point trajectory during multi-joint movement," *Biol. Cybern.*, vol. 76, no. 3, pp. 163–171, 1997.
[9] R. Osu and H. Gomi, "Multijoint muscle regulation mechanisms examined by measured human arm stiffness and EMG signals," *J. Neurophysiol.*, vol. 81, no. 4, pp. 1458–1468, 1999.
[10] S.-F. Chen and I. Kao, "Conservative congruence transformation for joint and cartesian stiffness matrices of robotic hands and fingers," *Int. J. Robot Res.*, vol. 19, no. 9, pp. 835–847, 2000.
[11] C. Ott, *Cartesian Impedance Control of Redundant and Flexible-joint Robots*. New York, NY, USA: Springer, 2008.
[12] A. Dietrich, C. Ott, and A. Albu-Schäffer, "An overview of null space projections for redundant, torque-controlled robots," *Int. J. Robot. Res.*, vol. 34, pp. 1385–1400, 2015.
[13] E. J. Perreault, R. F. Kirsch, and A. M. Acosta, "Multiple-input, multiple-output system identification for characterization of limb stiffness dynamics," *Biol. Cybern.*, vol. 80, no. 5, pp. 327–337, 1999.
[14] V. M. Zatsiorsky, *Kinetics of Human Motion*. Human Kinetics, Champaign, IL, USA, 2002.
[15] K. R. Holzbaur, W. M. Murray, and S. L. Delp, "A model of the upper extremity for simulating musculoskeletal surgery and analyzing neuromuscular control," *Ann. Biomed. Eng.*, vol. 33, no. 6, pp. 829–840, 2005.
[16] C. Fang, A. Ajoudani, N. Tsagarakis, and A. Bicchi, "A real-time identification and tracking method for the kinematic musculoskeletal model of human right arm," *IEEE Trans. Biomed. Eng.*, 2016, submitted for publication.
[17] G. Ettema, G. Styles, and V. Kippers, "The moment arms of 23 muscle segments of the upper limb with varying elbow and forearm positions: Implications for motor control," *Human Movement Sci.*, vol. 17, no. 2, pp. 201–220, 1998.
[18] D. Shin, J. Kim, and Y. Koike, "A myokinetic arm model for estimating joint torque and stiffness from EMG signals during maintained posture," *J. Neurophysiol.*, vol. 101, no. 1, pp. 387–401, 2009.
[19] E. Van Zuylen, C. Gielen, and J. D. Van Der Gon, "Coordination and inhomogeneous activation of human arm muscles during isometric torques," *J. Neurophysiol.*, vol. 60, no. 5, pp. 1523–1548, 1988.
[20] R. Osu and H. Gomi, "Multijoint muscle regulation mechanism examined by measured human arm stiffness and EMG signals," *J. Neurophysiol.*, vol. 81, pp. 1458–1468, 1999.
[21] A. Ajoudani, C. Fang, N. Tsagarakis, and A. Bicchi, "Reduced-complexity representation of the active arm endpoint stiffness for supervisory control of remote manipulation," *Int. J. Robot. Res.*, submitted for publication.
[22] A. Ajoudani, N. G. Tsagarakis, and A. Bicchi, "Tele-impedance: Teleoperation with impedance regulation using a body-machine interface," *Int. J. Robot. Res.*, pp. 1642–1655, 2012.